

Quantitative free-breathing dynamic contrast-enhanced MRI in hepatocellular carcinoma using gadoxetic acid: correlations with Ki67 proliferation status, histological grades, and microvascular density

Jie Chen,¹ Chenyang Chen,² Chunchao Xia,² Zixing Huang,² Panli Zuo,³ Alto Stemmer,⁴ Bin Song²

¹West China Medical School of Sichuan University, Chengdu 610041, Sichuan, China

²Department of Radiology, West China Hospital of Sichuan University, Guoxuexiang No. 37, Chengdu 610041, Sichuan province, China

³MR Collaboration NE Asia, Siemens Healthcare, Beijing 100000, China

⁴Siemens Healthcare, 91052 Erlangen, Germany

Abstract

Purpose: To validate a free-breathing dynamic contrast-enhanced-MRI (DCE-MRI) in hepatocellular carcinoma (HCC) patients using gadoxetic acid, and to determine the relationship between DCE-MRI parameters and histological results.

Methods: Thirty-four HCC patients were included in this prospective study. Free-breathing DCE-MRI data was acquired preoperatively on a 3.0 Tesla scanner. Perfusion parameters (K^{trans} , K_{ep} , V_e and the semi-quantitative parameter of initial area under the gadolinium concentration–time curve, iAUC) were calculated and compared with tumor enhancement at contrast-enhanced CT. The relationship between DCE-MRI parameters and Ki67 indices, histological grades and microvascular density (MVD) was determined by correlation analysis. Differences of perfusion parameters between different histopathological groups were compared. Receiver operation characteristic (ROC) analysis of discriminating high-grades (grade III and IV) from low-grades (grade I and II) HCC was performed for perfusion parameters.

Results: Significant relationship was found between DCE-MRI and CT results. The DCE-MRI derived K^{trans} were significantly negatively correlated with Ki-67 indices ($\rho = -0.408$, $P = 0.017$) and the histo-

logical grades ($\rho = -0.444$, $P = 0.009$) of HCC, and K_{ep} and V_e were significantly related with tumor MVD ($\rho = -0.405$, $P = 0.017$ for K_{ep} ; and $\rho = 0.385$, $P = 0.024$ for V_e). K^{trans} , K_{ep} , and iAUC demonstrated moderate diagnostic performance (iAUC = 0.78, 0.77 and 0.80, respectively) for discriminating high-grades from low-grades HCC without significant differences.

Conclusions: The DCE-MRI derived parameters demonstrated weak but significant correlations with tumor proliferation status, histological grades or microvascular density, respectively. This free-breathing DCE-MRI is technically feasible and offers a potential avenue toward non-invasive evaluation of HCC malignancy.

Key words: Dynamic contrast-enhanced magnetic resonance imaging—Hepatocellular carcinoma—Ki-67 proliferation—Histological grade—Microvascular density

Hepatocellular carcinoma (HCC) represents a major burden in clinical practice considering its high rate of morbidity and mortality [1]. Investigators have reported that the histological grade of HCC is a significant prognostic factor after surgery, with high-grade HCC associated with worse survival compared with low-grade HCC [2, 3]. The 5-year tumor-specific survival for Edmondson-Steiner grade I–II and grade III–IV were

81% and 18%, respectively, after curative resection in HCC patients without portal vein tumor thrombosis [4]. The Ki-67 proliferation index reflects the degree of proliferation activity and is significantly correlated with tumor grades [5]. In HCC, Ki67 expression was found to be in close relation to tumor growth rate [6] and was an independent prognostic indicator of patient disease-free and overall survival rates [7]. Recent study showed that the Ki67 expression level in HCC has a prognostic value similar with Edmonson-Steiner grading [8].

Tumor neovascularization is another important prognostic factor. Angiogenesis is a hallmark of tumor development and progression, which has been reported in the development of HCC [9, 10]. The hypervascular nature of this tumor suggested the importance of angiogenesis evaluation with the management and monitoring of HCC. The microvascular density (MVD), as assessed by CD31 or CD 34 staining, has generally been considered as an index of angiogenesis [11]. Clinical researches have revealed its correlation with histological grade and patient prognosis [12, 13]. However, despite their distinct prognostic significance, neither the histological grade nor MVD of HCCs is routinely available through biopsy for the invasiveness and concern of procedure-related complications [3].

Dynamic contrast-enhanced magnetic resonance imaging (DCE-MRI) in combination with pharmacokinetic modeling allows non-invasive evaluation of tumor malignancy and vascular physiology. To standardize the kinetic parameters derived from DCE-MRI, Tofts et al. proposed a model to quantitatively evaluate the perfusion parameters using the volume transfer constant (K^{trans}), the reflux rate constant (K_{ep}) and volume fraction (V_e) of the extravascular extracellular space (EES) per unit volume of tissue, where K^{trans} represents the volume transfer constant from blood plasma to EES, K_{ep} represent the rate constant from EES to blood plasma, and V_e is the volume of EES per unit volume of tissue [14]. Currently, this model has been successfully employed for tumor grading and treatment assessment in different organs, including brain, breast, pancreas and liver [15–19]. Conventional contrast-enhanced multiphase liver MRI is usually performed in multiple breath holds. However, when applying quantitative pharmacokinetic analysis, the multiphase DCE-MRI suffers from limited temporal and spatial resolution. Furthermore, these methods often provide no information on quantitative perfusion. Alternatively, a recently developed technique applying radial sampling with the golden-angle review order and contrast-enhancing k-space filter, currently named GOLD, was reported to be beneficial for free-breathing DCE-MRI with increased consistency in flip angles and decreased motion artifacts [20]. Moreover, although quantitative DCE-MRI has been frequently applied, the relationship between those perfusion parameters and histopathology has not yet been fully understood.

The purpose of this study was to explore the validity of a free-breathing DCE-MRI in HCC patients using gadoteric acid, by comparing it with contrast-enhanced computed tomography (CT), and to explore its clinical significance by correlating the DCE-MRI derived quantitative parameters with histological findings.

Materials and methods

Patients

This prospective study was approved by the Institutional Review Board. Written informed consent was obtained from all patients. The inclusion criteria were: (a) hepatic tumors suspected of HCC; (b) treatment-naïve; and (c) surgical resection was considered according to the clinical practice at local institution. Patients were considered not eligible if they were pregnant, under 18 years old or have contraindication to the liver-specific contrast agent enhanced MR examination (e.g., history of anaphylactoid reaction, renal failure, non-compatible biometallic implants or claustrophobia). A total of 40 patients were initially involved in this study. Three patients were excluded because the final pathology finding was confirmed not to be HCC. Three patients were additionally excluded owing to the failure to calculate the perfusion parameter because of massive necrosis in the tumor ($n = 2$) and severe motion artifact because of a left subphrenic location of the tumor ($n = 1$). Therefore, the final study group comprised 34 patients with a mean age of 54.82 ± 10.8 years (range 28–83 years). The mean time interval between MR examination and surgical resection was 1.97 ± 1.32 days (range 1–6 days). The underlying diseases of those HCC patients were hepatitis B ($n = 26$), both hepatitis B and C ($n = 1$), autoimmune hepatitis ($n = 1$), and cryptogenic disease ($n = 6$).

Image acquisition

Patients were examined using a 3.0T MR scanner (Magnetom Skyra, Siemens Healthcare, Erlangen, Germany) with an 18-channel phased-array body coil and spine coil within 1 week before surgery. All patients were asked to fast for 6 h before MR examination. High-spatial-resolution transverse and coronal T2-weighted images and transverse T1-weighted fat-suppressed MR images were acquired before contrast enhancement. Free-breathing DCE-MRI data were acquired using a prototype radial stack-of-stars three-dimensional (3D) spoiled gradient echo pulse sequence with golden-angle radial sampling schemes. The imaging parameters were as follows: TE/TR = 1.73/3.78 ms, flip angle = 12° , slice thickness = 1.5 mm, slices = 104, matrix = 256×256 , FOV = 380×380 mm². After baseline acquisition of 15 s, a dose of 0.025 mmol/kg Gd-EOB-DTPA (gadolinium ethoxybenzyl diethylenetriamine pentaacetic acid, Bayer Schering Pharma, Germany) was injected intravenously at a rate of

2 mL/sec via a power injector, followed by a 20 mL saline flush at the same rate. A total of 2108 radial spokes were acquired over the course of 6:15 min. Image reconstruction was performed on-line with a golden-angle view sharing technique [2]. K-space was divided into seven concentric rings filled with 34, 55, 89, 144, 233, 377, 610 spokes, respectively. The 34 spokes of the innermost ring correspond to a temporal resolution of approximately 6 s. Patients were asked to breathe slowly and smoothly during the acquisition process. After DCE-MRI acquisition, the hepatobiliary phase imaging was performed at 20 min after Gd-EOB-DTPA administration. All examination was conducted by the same technician with 15 years of experience in MR examination to reduce possible technical errors.

In twenty-nine patients, previous preoperative tri-phase dynamic contrast-enhanced CT was also performed. The scanning was performed using a dual source CT system (Somatom Definition; Siemens Healthcare, Forchheim, Germany) in a single tube mode with the following parameters: 120 kV, 200 mAs, rotation time of 0.5 s, collimation of 24×1.2 mm, pitch of 0.9, thickness of 5 mm, and gap of 2 mm. Contrast agent (iohexol, 300 mg iodine/mL; Bayer Schering Pharma AG, Leverkusen, Germany) dosed to weight (1.5 mL/kg) was injected at a rate of 2.5 mL/s with an automatic power injector after an initial unenhanced CT scanning. Arterial phase and portal venous phase were obtained around 30–35 s and 60–70 s after the contrast administration, considering the differences of patient's habitus and other factors. The time interval between CT and MR examination was 1.2 ± 0.8 days (range 1–4 days).

Image analysis

Post-processing of DCE-MRI data was performed on the Tissue-4D software (Siemens Healthcare) to calculate K^{trans} , K_{ep} , and V_e using a single-input two-compartment model based on the Toft's model [14]. An intermediate arterial input function (AIF) scale was adopted accordingly [21]. Initial area under the gadolinium concentration–time curve (iAUC) was also calculated. We measured both the mean (K^{trans} , K_{ep} , V_e and iAUC) and the maximum (max- K^{trans} , max- K_{ep} , max- V_e and max-iAUC) perfusion parameters of HCCs. For mean value quantification, a single representative region of interest (ROI) was traced manually along the margin of the tumor on the slice where tumors showed their largest transverse diameter on the pseudo-color images of perfusion parameters, avoiding areas of hemorrhage and necrosis by referring to the precontrast T1-weighted, T2-weighted, and dynamic contrast-enhanced T1-weighted images [22]. The average ROI size was 23.35 ± 16.84 cm² (range 2.16–71.85 cm²). A similarly sized ROI was placed on the background liver parenchyma (BLP), avoiding the inclusion of imaging artifacts and major vascular structures. To measure the maximum perfusion parameters, three additional ROIs were chosen at the hot spots of the pseudo-

color maps (i.e., most enhanced area) on the same slice of quantifying the mean parameters. This semi-automated measurement was conducted in consensus by two radiologists, who were blinded to histopathological results, and was repeated once. The average results of the two measurements were regarded as perfusion parameters.

All CT images were reviewed in consensus by the same two radiologists. To evaluate the enhancement degree of HCC, the CT attenuation values of the tumor were measured during the unenhanced, arterial and portal venous phase. A single representative ROI was carefully hand drawn to encircle the area identical to that of DCE-MRI parameters. The degree of arterial enhancement (AE) was defined as $[AE = (CT_{\text{arterial}} - CT_{\text{pre}})/CT_{\text{pre}}]$, and the degree of portal venous enhancement (PVE) was defined as $[PVE = (CT_{\text{portal}} - CT_{\text{pre}})/CT_{\text{pre}}]$, where CT_{arterial} and CT_{portal} are the CT attenuation values of HCC at arterial and portal venous phase, and CT_{pre} is the attenuation values at unenhanced CT.

Histopathological analysis

Tumor sections were matched as closely as possible to the lesion where the perfusion parameters were measured, i.e., the section where tumors showed their largest transverse diameter, using the transverse T2-weighted and contrast-enhanced T1-weighted images as reference. Resected specimens were fixed with 10% paraformaldehyde solution, embedded in paraffin and cut into 4 μ m-thick sections for either hematoxylin–eosin (H&E) staining or immunohistochemical identification of markers of proliferation (Ki-67 antigen) and MVD. Ki-67 (Rabbit monoclonal, SP6, Abcam, Cambridge, UK) (1:100 dilution) and anti-mouse CD31 (Rat monoclonal, MEC14.7, Abcam, Cambridge, UK) (1:50 dilution) staining was performed by standard avidin–biotin–peroxidase complex method and 3,3'-diaminobenzidine (DAB) solution was used for color development.

The histopathological examination was performed by an experienced pathologist with more than 10 years of experience, and was blinded to radiological and clinical results. The major histological grade of HCC (predominant grade within the tumor) was recorded according to Edmondson-Steiner classification [4], a long applied grading system for differentiation of HCC in that size and morphology of HCC cells, and was used for radiologic-pathologic correlation. Tumors with Edmondson-Steiner grade I and II were classified into low-grades group, while Edmondson-Steiner grade III and IV HCCs were classified into high-grades group. The Ki-67 labeling index was evaluated by calculating the rate of Ki-67 positive cells. To evaluate tumor angiogenesis, MVD was determined by examining the viable tumor area without necrosis, as described by previous studies [23, 24]. Briefly, the slides stained with CD31 were screened at

low power field ($\times 100$) and the five most vascular areas were selected for microvessel counts at high power field ($\times 400$). All positive stained cells were counted as microvessels. The average microvessel counts of selected areas were regarded as MVD.

Statistical analysis

Continuous variables are expressed as mean \pm standard deviation (SD). Scatterplots of DCE-MRI parameters and CT indices were generated. Where appropriate, Spearman's (or Pearson's) correlation analysis was used to identify a relationship between parameters of the two imaging modalities. Differences of DCE-MRI parameters between tumors and BLP were compared using non-parametric paired *t*-tests. Spearman's (or Pearson's) correlation analysis was performed to evaluate the correlation between perfusion parameters and histopathological results. An independent *t* test was used to compare perfusion parameters between different histopathological groups (high-groups of Ki67 index and MVD were defined higher than the median values). Receiver operation characteristic (ROC) analysis of discriminating low-grades from high-grades HCC was performed for perfusion parameters. Sensitivity and specificity with corresponding 95% confidence intervals (CI) were derived and areas under the ROC curve (AUC) were computed. Differences in diagnostic performances were analyzed by comparing the ROC curves according to the method of Delong et al. [25]. *P* values of less than 0.05 were regarded as statistically significant. All statistical analysis was carried out by commercially available MedCalc (MedCalc for Windows, version 11.5.0.0).

Results

Clinical and histopathological assessment

A total of 45 tumors were identified in the 34 patients. Among them, there were 26 patients with one lesion, five patients with two lesions, and three patients with more than two lesions. In patients with multifocal lesions, the largest lesion was chosen as the study target. The median tumor size was 5.8 cm (range 2.1–13.0 cm). The median AFP level was 116.35 ng/ml (range 1.29–26,282 ng/ml). The 34 selected HCCs were histopathologically classified according to the major Edmondson-Steiner grade. MVD and Ki67 index were determined as previously described. The clinical and hispathological information was summarized in Table 1.

Comparison of DCE-MRI and CT results

Figure 1 shows the scatterplots of median values of AE and PVE vs. median values of K^{trans} and iAUC. Correlation analysis demonstrated significant relationship between DCE-MRI parameters and CT indices. Both K^{trans} and

Table 1. Patients and tumor characteristics

Characteristics	Value
Age (years)	Mean \pm SD: 54.82 \pm 10.8 (range 28–83)
Male/female	24/10
AFP (ng/ml) ^a	Median: 116.35 (range 1.29–26,282)
Underlying liver disease	
Hepatitis B	26
Hepatitis B and C	1
Autoimmune hepatitis	1
Cryptogenic	6
Tumor size (cm)	Median: 5.8 (range 2.1–13.0)
Edmondson-Steiner grade	
Low-grades	19
Grade I	4
Grade II	15
High-grades	15
Grade III	11
Grade IV	4
Microvascular density	Mean \pm SD: 29.12 \pm 13.94 vessels/field (range 4.8–54.2)
Ki67 index	Median: 24.55% (range 1.21%–86%)

^a Normal values for serum AFP are under 8 ng/ml
AFP, alpha-fetoprotein; SD, standard deviation

iAUC were significantly correlated with AE and PVE of HCC ($\rho = 0.549$, $P = 0.002$ for K^{trans} vs. AE, and $\rho = 0.447$, $P = 0.015$ for K^{trans} vs. PVE; $\rho = 0.546$, $P = 0.002$ for iAUC vs. AE, and $\rho = 0.558$, $P = 0.002$ for iAUC vs. PVE). No significant correlation with AE and PVE was observed for K_{ep} and V_e ($P > 0.05$ for all).

Quantitative perfusion parameters

The K^{trans} , K_{ep} , V_e , and iAUC were $0.57 \pm 0.32 \text{ min}^{-1}$, $2.31 \pm 1.41 \text{ min}^{-1}$, 0.32 ± 0.1 , and 5.55 ± 2.14 for HCC; and $0.23 \pm 0.07 \text{ min}^{-1}$, $0.61 \pm 0.28 \text{ min}^{-1}$, 0.43 ± 0.11 , and 3.21 ± 0.75 for BLP. The K^{trans} , K_{ep} , and iAUC of HCC were significantly higher than that of BLP ($P < 0.001$ for all), and the V_e of HCC was significantly lower than that of BLP ($P < 0.001$).

Correlation between perfusion parameters and histopathological results

A significant negative correlation between K^{trans} and the Ki67 index was observed ($\rho = -0.408$, $P = 0.017$) (Fig. 2), no significant correlation was found between the maximum perfusion parameters and Ki67 index ($P > 0.05$ for all). The K^{trans} and iAUC were significantly correlated with the Edmondson-Steiner grade of HCC ($\rho = -0.444$, $P = 0.009$ for K^{trans} , and $\rho = -0.523$, $P = 0.002$ for iAUC), while no significant correlation with the histological grade was observed for K_{ep} and V_e ($P > 0.05$ for all). As to the maximum parameters, only the max- K^{trans} was correlated with tumor grades ($\rho = -0.382$, $P = 0.028$). The K^{trans} , K_{ep} , and iAUC of high-grades HCC were significantly lower than that of low-grades HCC ($P = 0.001$, 0.031 , and

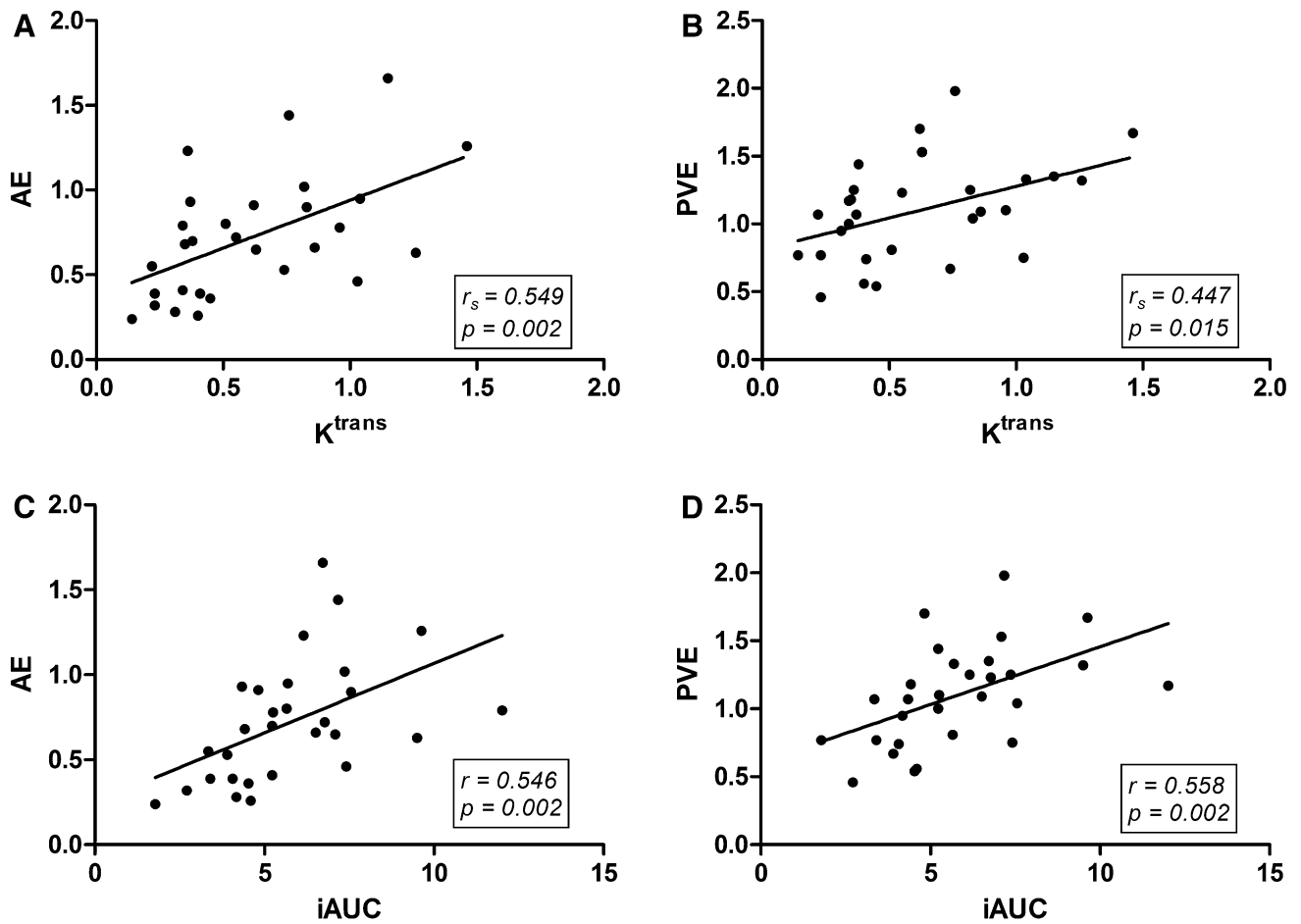


Fig. 1. Scatterplots of the comparison of the median values of K^{trans} and iAUC vs. tumor arterial enhancement (AE) and portal venous enhancement (PVE) degree. Significant positive correlation was demonstrated between K^{trans} , iAUC, and AE and PVE of HCC.

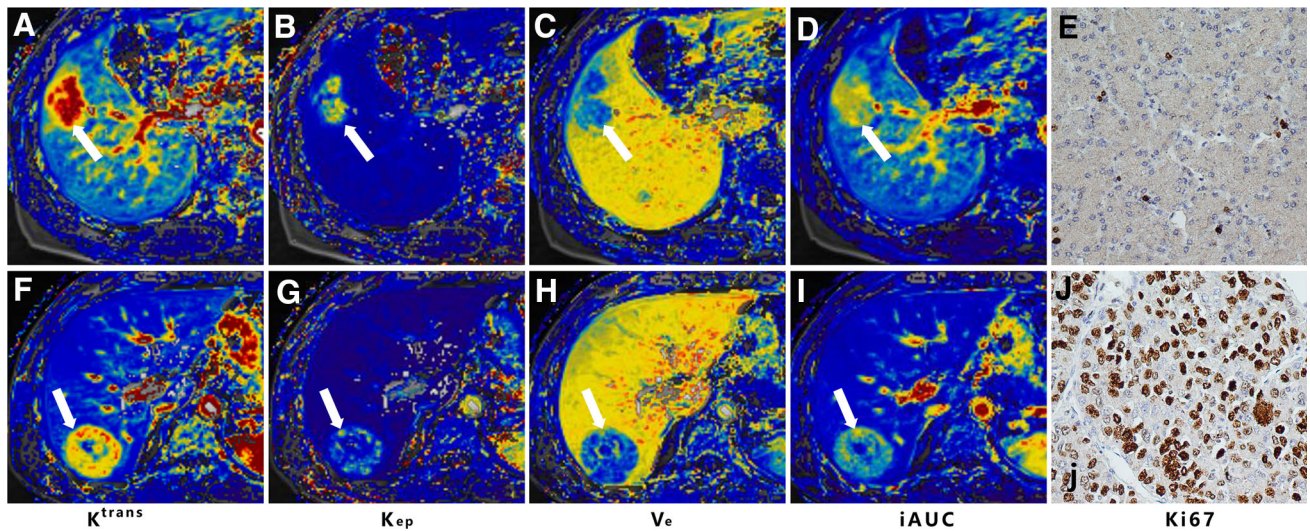


Fig. 2. Representative perfusion images of a poorly proliferative (A–D) and highly proliferative (F–I) HCC, as indicated by the Ki67 index. HCC with higher K^{trans} (A) was

correlated with lower Ki67 index (E). Other perfusion parameters did not differ significantly between Ki67 low- and high-groups.

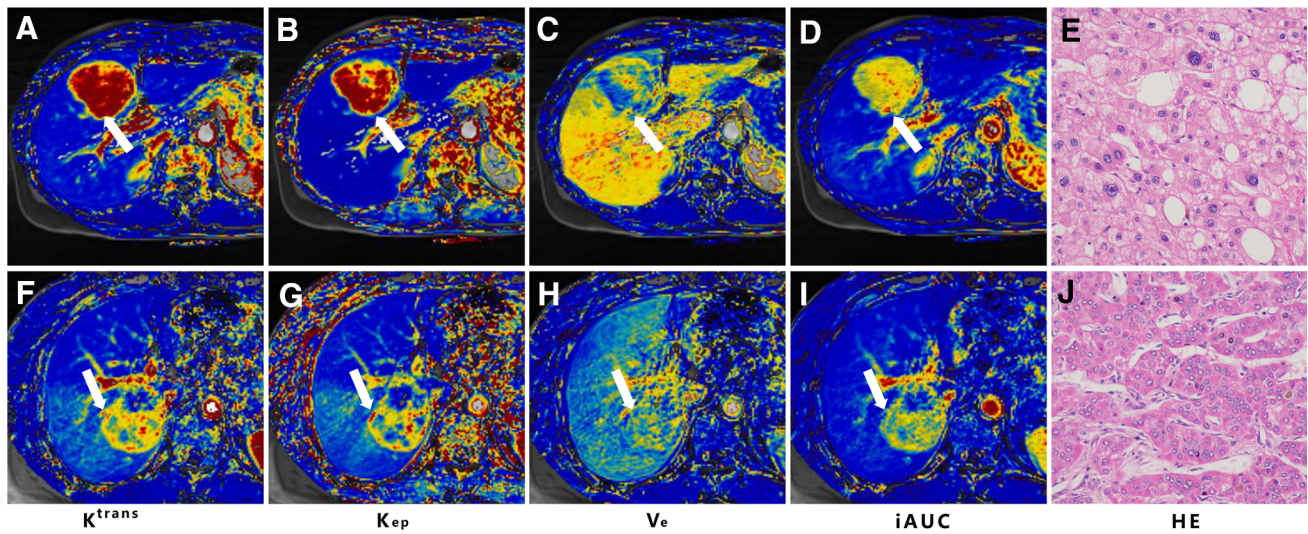


Fig. 3. Representative perfusion images of a low-grade (A–D) and high-grade (F–I) HCC. K^{trans} and iAUC were significantly negatively correlated with tumor differentiation. The K^{trans} (F vs. A), K_{ep} (G vs. B), and iAUC (I vs. D) of high-grade HCC were significantly lower than that of low-grade HCC, but there was no statistically significant difference for V_e between the two groups.

Table 2. Correlations between perfusion parameters and histopathological results

	Ki67 index		Edmondson-Steiner grades		MVD	
	Mean	Max	Mean	Max	Mean	Max
K^{trans} (min^{-1})	-0.408*	-0.232	-0.444**	-0.382*	-0.195	-0.317
K_{ep} (min^{-1})	-0.183	-0.098	-0.336	-0.266	-0.405*	-0.445**
V_e	-0.291	-0.149	-0.233	-0.234	0.385*	0.419*
iAUC	-0.243	-0.053	-0.523**	-0.292	0.230	0.098

Values are statistically significant at ** $P \leq 0.01$ and at * $P \leq 0.05$

K^{trans} , volume transfer constant; K_{ep} , reflux rate; V_e , extravascular extracellular space; iAUC, initial area under the gadolinium concentration–time curve; MVD, microvascular density

Table 3. The comparison of mean perfusion parameters between different histopathological groups

	Ki67 index			Edmondson-Steiner grades			MVD		
	Low-group ($N = 17$)	High-group ($N = 17$)	P	Low-grades ($N = 19$)	High-grades ($N = 15$)	P	Low-group ($N = 15$)	High-group ($N = 19$)	P
K^{trans} (min^{-1})	0.70 ± 0.34	0.45 ± 0.25	0.019	0.72 ± 0.35	0.39 ± 0.15	0.001	0.60 ± 0.27	0.55 ± 0.36	0.698
K_{ep} (min^{-1})	2.71 ± 1.58	1.91 ± 1.13	0.101	2.77 ± 1.37	1.73 ± 1.28	0.031	2.91 ± 1.54	1.84 ± 1.13	0.026
V_e	0.34 ± 0.11	0.30 ± 0.10	0.256	0.32 ± 0.11	0.30 ± 0.10	0.59	0.27 ± 0.07	0.36 ± 0.11	0.009
iAUC	6.04 ± 1.86	5.05 ± 2.34	0.181	6.48 ± 2.24	4.37 ± 1.29	0.003	4.94 ± 1.41	6.03 ± 2.51	0.120

K^{trans} , volume transfer constant; K_{ep} , reflux rate; V_e , extravascular extracellular space; iAUC, initial area under the gadolinium concentration–time curve; MVD, microvascular density

0.003, respectively), but there was no statistically significant differences for V_e between the two groups ($P > 0.05$)(Fig. 3). Among those clinical characteristics, only the serum level of AFP was significantly correlated with tumor histological grade ($\rho = 0.508$, $P = 0.002$). Table 2 shows the correlation between perfusion parameters and histopathological results. The comparison of each perfusion parameter between different groups was demonstrated in Table 3.

With regard to the microvasculature, both the mean and the maximum K_{ep} and V_e of HCC were correlated significantly with MVD ($\rho = -0.405$, $P = 0.017$ for K_{ep} and $\rho = -0.445$, $P = 0.009$ for max- K_{ep} ; $r = 0.385$, $P = 0.024$ for V_e and $r = 0.419$, $P = 0.015$ for max- V_e) (Fig. 4), while K^{trans} and iAUC did not correlate with MVD. Patients' age, gender ratio, tumor size, and the level of serum alpha-fetoprotein were not correlated with MVD.

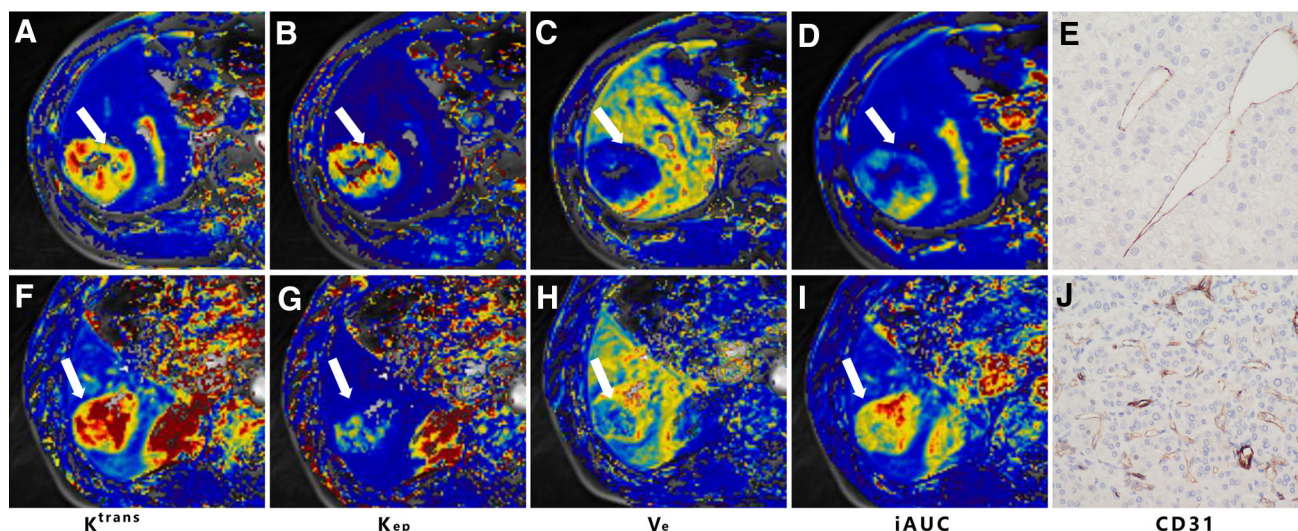


Fig. 4. Representative perfusion images of a poorly vascularized (**A–D**) and highly vascularized (**F–I**) HCC, as indicated by the microvascular density (MVD). HCC with lower K_{ep}

(**G**) and higher V_e (**H**) was significantly associated with higher MVD (**J**). Other perfusion parameters did not differ significantly between MVD low- and high-groups.

ROC analysis of discriminating low-grade from high-grade HCC

The diagnostic sensitivity and specificity with corresponding 95% CI of discriminating low-grades from high-grades HCC was 93.3% (68.1%–99.8%) and 63.2% (38.4%–83.7%) for K^{trans} , 86.7% (59.5%–98.3%) and 73.7% (48.8%–90.9%) for K_{ep} , and 73.3% (44.9%–92.2%) and 78.9% (54.4%–93.9%) for iAUC. The areas under ROC curve (AUC) of K^{trans} , K_{ep} , and iAUC were 0.78 (0.60–0.90), 0.77 (0.59–0.89), and 0.80 (0.63–0.92), respectively. There were no significant differences between the diagnostic performances of each parameter ($P > 0.05$ for all). The ROC curves of K^{trans} , K_{ep} , and iAUC for discriminating low-grades from high-grades HCC is shown in Fig. 5.

Discussion

With the radial acquisition with golden-angle scheme, we performed a free-breathing quantitative DCE-MRI for liver imaging. Vascular changes in HCC can be reliably detected and quantified by this method without distinct motion artifact. The relationships between DCE-MRI and CT results could suggest the validity of this method in evaluating the vascular changes of HCC. The increased K^{trans} was considered to reflect an increased vascular permeability in HCC, and the decreased V_e , which was mainly determined by the interstitial distribution space, indicated an aggressive growth of tumor cells [19, 26].

Tumors with higher ki67 indices tend to have relatively lower K^{trans} values. Further exploration revealed a negative and weak correlation between K^{trans} , iAUC, and

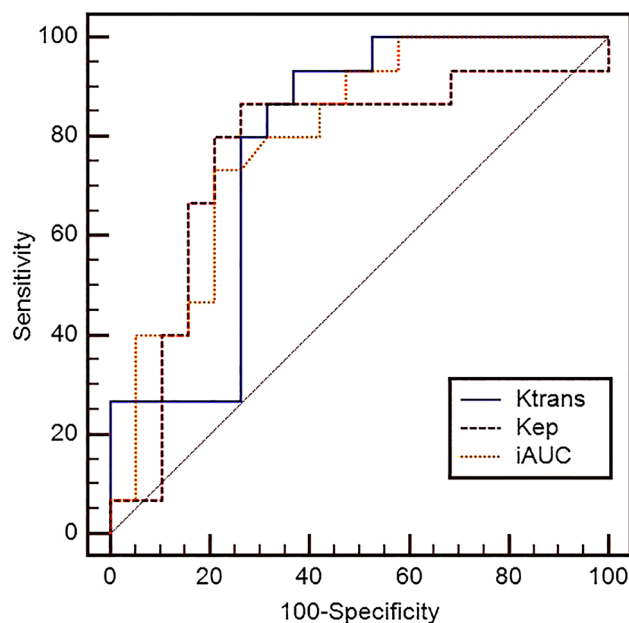


Fig. 5. The ROC curves of K^{trans} , K_{ep} , and iAUC for discriminating low-grades from high-grades HCC. There were no significant differences between the diagnostic performances of each parameter.

tumor histological grade. The mean perfusion parameters correlate better with Ki67 index and Edmondson-Steiner grade compared with the maximum perfusion parameters. ROC analysis demonstrated moderate diagnostic performance for K^{trans} , K_{ep} , and iAUC for discriminating high-grades from low-grades HCC. Although no significant differences were found between the diagnostic performances of each index, K^{trans} shows the

highest sensitivity (93.3%), while the best specificity (78.9%) was achieved by iAUC.

Of the various perfusion parameters, K^{trans} is the most commonly used DCE-MRI parameters. It reflects a combination of blood flow, vessel permeability, and vessel density [14]. In addition, the semi-quantitative parameter, iAUC, is associated with tumor blood influx, perfusion, and interstitium, representing the general tumor blood flow, overall perfusion, and tumor interstitial space index [14]. It is a relatively robust and simple kinetic parameter to derive and is able to characterize all enhancing regions without problems associated with model fitting failures [27]. Therefore, K^{trans} and iAUC were expected to better represent the actual vascular features of HCC than other parameters. The results that both K^{trans} and iAUC were correlated significantly with the histological grade of HCC in the present study suggested the potential of those parameters in predicting the malignancy of tumors. On the other hand, neither K_{ep} nor V_e were significantly associated with tumor differentiation. Shen et al. [28] speculated that because K_{ep} and V_e were related with the composition of EES, and despite the increased local vascular permeability, the composition of EES did not differ markedly among lesions with different differentiation statuses.

Quantitative assessment of tumor perfusion characteristics based on DCE-MRI was found to be correlated with tumor proliferation, tumor differentiation, and/or patient prognosis in many studies [28–31]. Inconsistent with those findings, our results revealed a negative correlation between K^{trans} , Ki67 index, and histologic grade. We speculate this discrepancy might be due to the adoption of different post-processing model and the hepatocyte-specific contrast agent of Gd-EOB-DTPA in this study. It remains unclear why K^{trans} is correlated with Ki67 proliferation status and histological grade in HCC, but there are some favorable results. Longer progression-free survivals were reported to be associated with higher baseline perfusion parameters such as K^{trans} in HCC [30] and renal cell carcinoma [32] patients. Those conclusions are in keeping with our results, i.e., higher baseline K^{trans} is a predictive marker of favorable biological behavior. Barnes et al. [33] hypothesized a direct relationship between K^{trans} and proliferation by observing a potential spatial correlation between the parametric maps of K^{trans} , AUC, and SUV from ^{18}F -FLT PET, but this hypothesis needs further exploration.

In terms of microvasculature, we found that lower K_{ep} and higher V_e were associated with higher MVD, while K^{trans} and iAUC were not correlated with MVD. The best correlation between MVD and perfusion parameters was found with the adoption of maximum parameters. Over the last few years, many studies have attempted to correlate tumor MVD with DCE-MRI derived K^{trans} , K_{ep} , and V_e with greatly varied results [34–

38], but few studies have focused on HCC. Results of the present study contradict with that of previous studies. Such inconsistent results may be attributed to differences among study groups and the endothelial markers employed to quantify MVD, for the positive correlation was found with the use of a newly identified CD105 as a marker of endothelial cells highly involved in the process of tumor angiogenesis. Another explanation could also be the adoption of the hepatocyte-specific contrast agent of Gd-EOB-DTPA. Besides, there are researchers [39, 40] who think that a lack of correlation between DCE-MRI parameters and histology does not necessarily suggest inaccuracy of the parameter, but perhaps that the complex and continuously changing metabolic demands of tumor angiogenesis is not adequately sampled by histological techniques.

High-grade HCC was found to an independent predictor of microvascular invasion [41], and was associated with early recurrence and worse survival [4]. For this reason, careful assessment is required in patients with high-grade HCC when surgical plan was considered [42]. The changes in tumor MVD were also frequently employed in evaluating treatment response [24, 37, 43]. Preoperative HCC characterization is therefore pivotal to treatment planning, prognosis prediction, as well as drug selection. Current technique advances in MRI have enabled HCC malignancy characterization through diffusion-weighted imaging [44, 45], DCE-MRI [44, 46], hepatobiliary phase [47, 48], and the recently reported magnetic resonance elastography [49]. Among them, DCE-MRI was expected to provide more information. In combination with gadoteric acid, this DCE-MRI can provide perfusion and hepatobiliary information at one-stop examination, enabling combined tumor diagnosis, and evaluation. The weak correlation between DCE-MRI parameters and histopathological results in this study implied the potential of this DCE-MRI protocol in preoperatively and non-invasively characterizing HCC.

The major argument about this study should be the application of the single-input model during post-processing. Normally, liver has dual blood supply and a dual input model is favored [19]. But things are slightly different in HCC. According to early researches [50, 51], during multistep hepatocarcinogenesis of HCC, the intranodular arterial supply first decreases at the early stage and then acutely increases, and finally, the entire nodule is fed only by the abnormal hepatic artery. Currently, there is no consensus as to which kinetic model is best suited [19]. Because HCC receives major blood supply from hepatic arteries, the single-input model was commonly used in many articles [19, 20] and in this study.

Another issue is the adoption of the hepatocyte-specific contrast agent of Gd-EOB-DTPA. Gd-EOB-DTPA is a chelate of albumin and Gd-DTPA, allowing

Gd-DTPA reversible and non-covalent binding to protein to prolong intravascular persistence [52]. Among the last few years, the liver-specific contrast agent Gd-EOB-DTPA has shown different characteristics from traditional gadolinium-based contrast media in DCE-MRI [53, 54]. Besides, as a liver-specific contrast agent, Gd-EOB-DTPA is also accumulated and excreted through the bile ducts. Therefore, the use of the Toft's model in this study may not be valid. It's worth noting that, according to previously established conclusion [55, 56], the cellular uptake of Gd-EOB-DTPA in HCC was dramatically decreased due to decreased membranal expression of the uptake transporter organic anion-transporting polypeptide 8 (OATP8). This, we assume could ease the concern to some extent. Though efforts have been reported in establishing specialized post-processing model for DCE-MRI using Gd-EOB-DTPA [57, 58], no consensus has been reached. The development of a generally recognized model is necessary to enable the combined tumor detection and evaluation.

Several other limitations about our study should also be acknowledged. First, although we included only HCC patients, the patient numbers were small, and the radiologic-pathologic correlation was all based on surgical specimens, thus may bring a selection bias. Second, we did not assess the intraindividual variability of those pharmacokinetic parameters, which is clinically important when DCE-MRI is involved in monitoring of treatment response. Third, the hepatocyte-specific contrast media of Gd-EOB-DTPA was used in this study. Although different perfusion characteristics of Gd-EOB-DTPA have been previously reported, we fail to further explore the influence of Gd-EOB-DTPA on the pharmacokinetic parameters compared with traditional gadolinium-based contrast media in this study. Moreover, we did not explore possible correlations between baseline DCE-MRI parameters and long-term clinical outcomes. Also, the accuracy of the DCE-MRI parameters is influenced by magnitude of motion artifact; therefore, the application of this protocol in lesions with subphrenic location is limited. Further investigations are required in a larger patient cohort to confirm these preliminary results and to validate the clinical utility of our work.

In conclusion, this free-breathing quantitative DCE-MRI protocol provides a valid and practicable method for future liver perfusion imaging. The DCE-MRI derived K^{trans} were significantly correlated with Ki-67 proliferation status and the histological grade of HCC, and K_{ep} and V_e were correlated with tumor MVD. The weak correlations between DCE-MRI parameters and histological results offer a potential avenue toward non-invasive evaluation of HCC malignancy.

Acknowledgement This study was funded by National Natural Science Foundation of China (Grant Number 81471658).

Compliance with ethical standards

Conflict of interest Author Jie Chen declares that she has no conflict of interest. Author Chenyang Chen declares that she has no conflict of interest. Author Chunchao Xia declares that he has no conflict of interest. Author Zixing Huang declares that he has no conflict of interest. Author Panli Zuo declares that she has no conflict of interest. Author Alto Stemmer declares that he has no conflict of interest. Author Bin Song declares that he has no conflict of interest.

Ethical approval All procedures performed in studies involving human participants were in accordance with the ethical standards of the institutional and/or national research committee and with the 1964 Helsinki declaration and its later amendments or comparable ethical standards. Informed consent was obtained from all individual participants included in the study.

References

1. Siegel RL, Miller KD, Jemal A (2015) Cancer statistics, 2015. *CA Cancer J Clin* 65:5–29
2. Jonas S, Bechstein WO, Steinmuller T, et al. (2001) Vascular invasion and histopathologic grading determine outcome after liver transplantation for hepatocellular carcinoma in cirrhosis. *Hepatology* 33:1080–1086
3. Perez-Saborido B, De Los Galanes SJ, Meneu-Diaz JC, et al. (2007) Tumor recurrence after liver transplantation for hepatocellular carcinoma: recurrence pathway and prognostic factors. *Transplant Proc* 39:2304–2307
4. Zhou L, Rui JA, Wang SB, Chen SG, Qu Q (2015) Clinicopathological predictors of poor survival and recurrence after curative resection in hepatocellular carcinoma without portal vein tumor thrombosis. *Pathol Oncol Res* 21:131–138
5. D'Errico A, Grigioni WF, Fiorentino M, et al. (1994) Overexpression of p53 protein and Ki67 proliferative index in hepatocellular carcinoma: an immunohistochemical study on 109 Italian patients. *Pathol Int* 44:682–687
6. Hsu HC, Tseng HJ, Lai PL, Lee PH, Peng SY (1993) Expression of p53 gene in 184 unifocal hepatocellular carcinomas: association with tumor growth and invasiveness. *Cancer Res* 53:4691–4694
7. Nigro JM, Baker SJ, Preisinger AC, et al. (1989) Mutations in the p53 gene occur in diverse human tumour types. *Nature* 342:705–708
8. Stroescu C, Dragnea A, Ivanov B, et al. (2008) Expression of p53, Bcl-2, VEGF, Ki67 and PCNA and prognostic significance in hepatocellular carcinoma. *J Gastrointest Liver Dis* 17:411–417
9. Yamaguchi R, Yano H, Iemura A, et al. (1998) Expression of vascular endothelial growth factor in human hepatocellular carcinoma. *Hepatology* 28:68–77
10. Zhang W, Kim R, Quintini C, et al. (2015) Prognostic role of plasma vascular endothelial growth factor in patients with hepatocellular carcinoma undergoing liver transplantation. *Liver Transpl* 21:101–111
11. Mann CD, Neal CP, Garcea G, et al. (2007) Prognostic molecular markers in hepatocellular carcinoma: a systematic review. *Eur J Cancer* 43:979–992
12. Murakami K, Kasajima A, Kawagishi N, Ohuchi N, Sasano H (2015) Microvessel density in hepatocellular carcinoma: Prognostic significance and review of the previous published work. *Hepatology* 45:1185–1194
13. Li Y, Ma X, Zhang J, Liu X, Liu L (2014) Prognostic value of microvessel density in hepatocellular carcinoma patients: a meta-analysis. *Int J Biol Markers* 29:e279–e287
14. Tofts PS, Brix G, Buckley DL, et al. (1999) Estimating kinetic parameters from dynamic contrast-enhanced T(1)-weighted MRI of a diffusible tracer: standardized quantities and symbols. *J Magn Reson Imaging* 10:223–232
15. Yang X, Knopp MV (2011) Quantifying tumor vascular heterogeneity with dynamic contrast-enhanced magnetic resonance imaging: a review. *J Biomed Biotechnol* 2011:732848
16. Rao SX, Chen CZ, Liu H, Zeng MS, Qu XD (2013) Three-dimensional whole-liver perfusion magnetic resonance imaging in patients with hepatocellular carcinoma and colorectal hepatic metastases. *BMC Gastroenterol* 13:53

17. Huh J, Choi Y, Woo DC, et al. (2016) Feasibility of test-bolus DCE-MRI using CAIPIRINHA-VIBE for the evaluation of pancreatic malignancies. *Eur Radiol*. doi:10.1007/s00330-016-4209-6
18. Hao W, Zhao B, Wang G, Wang C, Liu H (2015) Influence of scan duration on the estimation of pharmacokinetic parameters for breast lesions: a study based on CAIPIRINHA-Dixon-TWIST-VIBE technique. *Eur Radiol* 25:1162–1171
19. Chen BB, Shih TT (2014) DCE-MRI in hepatocellular carcinoma-clinical and therapeutic image biomarker. *World J Gastroenterol* 20:3125–3134
20. Braren R, Curcic J, Remmele S, et al. (2011) Free-breathing quantitative dynamic contrast-enhanced magnetic resonance imaging in a rat liver tumor model using dynamic radial T(1) mapping. *Invest Radiol* 46:624–631
21. FritzHansen T, Rostrup E, Larsson HBW, et al. (1996) Measurement of the arterial concentration of Gd-DTPA using MRI: a step toward quantitative perfusion imaging. *Magn Reson Med* 36:225–231
22. Wagner M, Doblaz S, Daire JL, et al. (2012) Diffusion-weighted MR imaging for the regional characterization of liver tumors. *Radiology* 264:464–472
23. Shinriki S, Jono H, Ota K, et al. (2009) Humanized anti-interleukin-6 receptor antibody suppresses tumor angiogenesis and in vivo growth of human oral squamous cell carcinoma. *Clin Cancer Res* 15:5426–5434
24. Song KD, Choi D, Lee JH, et al. (2014) Evaluation of tumor microvascular response to brivanib by dynamic contrast-enhanced 7-T MRI in an orthotopic xenograft model of hepatocellular carcinoma. *AJR Am J Roentgenol* 202:W559–W566
25. DeLong ER, DeLong DM, Clarke-Pearson DL (1988) Comparing the areas under two or more correlated receiver operating characteristic curves: a nonparametric approach. *Biometrics* 44:837–845
26. Zwick S, Brix G, Tofts PS, et al. (2010) Simulation-based comparison of two approaches frequently used for dynamic contrast-enhanced MRI. *Eur Radiol* 20:432–442
27. Padhani AR, Khan AA (2010) Diffusion-weighted (DW) and dynamic contrast-enhanced (DCE) magnetic resonance imaging (MRI) for monitoring anticancer therapy. *Target Oncol* 5:39–52
28. Shen FU, Lu J, Chen L, Wang Z, Chen Y (2016) Diagnostic value of dynamic contrast-enhanced magnetic resonance imaging in rectal cancer and its correlation with tumor differentiation. *Mol Clin Oncol* 4:500–506
29. Wegner CS, Gaustad JV, Andersen LM, Simonsen TG, Rofstad EK (2016) Diffusion-weighted and dynamic contrast-enhanced MRI of pancreatic adenocarcinoma xenografts: associations with tumor differentiation and collagen content. *J Transl Med* 14:161
30. Kim KA, Park MS, Ji HJ, et al. (2014) Diffusion and perfusion MRI prediction of progression-free survival in patients with hepatocellular carcinoma treated with concurrent chemoradiotherapy. *J Magn Reson Imaging* 39:286–292
31. Shin JK, Kim JY (2017) Dynamic contrast-enhanced and diffusion-weighted MRI of estrogen receptor-positive invasive breast cancers: Associations between quantitative MR parameters and Ki-67 proliferation status. *J Magn Reson Imaging* 45:94–102
32. Flaherty KT, Rosen MA, Heitjan DF, et al. (2008) Pilot study of DCE-MRI to predict progression-free survival with sorafenib therapy in renal cell carcinoma. *Cancer Biol Ther* 7:496–501
33. Barnes SL, Whisenant JG, Loveless ME, Yankeelov TE (2012) Practical dynamic contrast enhanced MRI in small animal models of cancer: data acquisition, data analysis, and interpretation. *Pharmaceutics* 4:442–478
34. Kim YE, Lim JS, Choi J, et al. (2013) Perfusion parameters of dynamic contrast-enhanced magnetic resonance imaging in patients with rectal cancer: correlation with microvascular density and vascular endothelial growth factor expression. *Korean J Radiol* 14:878–885
35. Li L, Wang K, Sun X, et al. (2015) Parameters of dynamic contrast-enhanced MRI as imaging markers for angiogenesis and proliferation in human breast cancer. *Med Sci Monit* 21:376–382
36. Jia ZZ, Gu HM, Zhou XJ, et al. (2015) The assessment of immature microvascular density in brain gliomas with dynamic contrast-enhanced magnetic resonance imaging. *Eur J Radiol* 84:1805–1809
37. Chen J, Qian T, Zhang H, et al. (2016) Combining dynamic contrast enhanced magnetic resonance imaging and microvessel density to assess the angiogenesis after PEI in a rabbit VX2 liver tumor model. *Magn Reson Imaging* 34:177–182
38. Bali MA, Metens T, Denolin V, et al. (2011) Tumoral and nontumoral pancreas: correlation between quantitative dynamic contrast-enhanced MR imaging and histopathologic parameters. *Radiology* 261:456–466
39. Mayr NA, Hawighorst H, Yuh WT, et al. (1999) MR microcirculation assessment in cervical cancer: correlations with histomorphological tumor markers and clinical outcome. *J Magn Reson Imaging* 10:267–276
40. Cheng HL, Wallis C, Shou Z, Farhat WA (2007) Quantifying angiogenesis in VEGF-enhanced tissue-engineered bladder constructs by dynamic contrast-enhanced MRI using contrast agents of different molecular weights. *J Magn Reson Imaging* 25:137–145
41. Kim BK, Han KH, Park YN, et al. (2008) Prediction of microvascular invasion before curative resection of hepatocellular carcinoma. *J Surg Oncol* 97:246–252
42. Oishi K, Itamoto T, Amano H, et al. (2007) Clinicopathologic features of poorly differentiated hepatocellular carcinoma. *J Surg Oncol* 95:311–316
43. Qian T, Chen M, Gao F, et al. (2014) Diffusion-weighted magnetic resonance imaging to evaluate microvascular density after transarterial embolization ablation in a rabbit VX2 liver tumor model. *Magn Reson Imaging* 32:1052–1057
44. An C, Park MS, Jeon HM, et al. (2012) Prediction of the histopathological grade of hepatocellular carcinoma using qualitative diffusion-weighted, dynamic, and hepatobiliary phase MRI. *Eur Radiol* 22:1701–1708
45. Chang WC, Chen RC, Chou CT, et al. (2014) Histological grade of hepatocellular carcinoma correlates with arterial enhancement on gadoteric acid-enhanced and diffusion-weighted MR images. *Abdom Imaging* 39:1202–1212
46. Choi YS, Rhee H, Choi JY, et al. (2013) Histological characteristics of small hepatocellular carcinomas showing atypical enhancement patterns on gadoteric acid-enhanced MR imaging. *J Magn Reson Imaging* 37:1384–1391
47. Kogita S, Imai Y, Okada M, et al. (2010) Gd-EOB-DTPA-enhanced magnetic resonance images of hepatocellular carcinoma: correlation with histological grading and portal blood flow. *Eur Radiol* 20:2405–2413
48. Tahir B, Sandrasegaran K, Ramaswamy R, et al. (2011) Does the hepatocellular phase of gadobenate dimeglumine help to differentiate hepatocellular carcinoma in cirrhotic patients according to histological grade? *Clin Radiol* 66:845–852
49. Thompson SM, Wang J, Chandan VS, et al. (2017) MR elastography of hepatocellular carcinoma: Correlation of tumor stiffness with histopathology features-Preliminary findings. *Magn Reson Imaging* 37:41–45
50. Matsui O, Kobayashi S, Sanada J, et al. (2011) Hepatocellular nodules in liver cirrhosis: hemodynamic evaluation (angiography-assisted CT) with special reference to multi-step hepatocarcinogenesis. *Abdom Imaging* 36:264–272
51. Park YN, Yang CP, Fernandez GJ, et al. (1998) Neoangiogenesis and sinusoidal “capillarization” in dysplastic nodules of the liver. *Am J Surg Pathol* 22:656–662
52. Kiessling F, Morgenstern B, Zhang C (2007) Contrast agents and applications to assess tumor angiogenesis in vivo by magnetic resonance imaging. *Curr Med Chem* 14:77–91
53. Wu L, Lv P, Zhang H, et al. (2015) Dynamic contrast-enhanced (DCE) MRI assessment of microvascular characteristics in the murine orthotopic pancreatic cancer model. *Magn Reson Imaging* 33:737–760
54. Lin YH, Hwang RM, Chen BB, et al. (2014) Vascular and hepatic enhancements at MR imaging: comparison of Gd-EOB-DTPA and Gd-DTPA in the same subjects. *Clin Imaging* 38:287–291
55. Narita M, Hatano E, Arizono S, et al. (2009) Expression of OATP1B3 determines uptake of Gd-EOB-DTPA in hepatocellular carcinoma. *J Gastroenterol* 44:793–798
56. Kitao A, Matsui O, Yoneda N, et al. (2011) The uptake transporter OATP8 expression decreases during multistep hepatocarcinogenesis: correlation with gadoteric acid enhanced MR imaging. *Eur Radiol* 21:2056–2066

57. Sourbron S, Sommer WH, Reiser MF, Zech CJ (2012) Combined quantification of liver perfusion and function with dynamic gadoteric acid-enhanced MR imaging. *Radiology* 263:874–883
58. Nilsson H, Nordell A, Vargas R, et al. (2009) Assessment of hepatic extraction fraction and input relative blood flow using dynamic hepatocyte-specific contrast-enhanced MRI. *J Magn Reson Imaging* 29:1323–1331